

1 **Formation of fluorohydroxyapatite with silver diamine fluoride**

2
3 **May L. Mei¹, Fabio Nudelman², Bartosz Marzec², Jessica M. Walker², Edward**
4 **C. M. Lo¹, Angus W. Walls^{3*}, C. H. Chu^{1*}**

5
6 ¹ Faculty of Dentistry, The University of Hong Kong, Hong Kong SAR, China

7
8 ² EaStCHEM, School of Chemistry, The University of Edinburgh, Joseph Black Building, David
9 Brewster Road, Edinburgh EH9 3FJ, United Kingdom

10
11 ³ Edinburgh Dental Institute, The University of Edinburgh, Edinburgh, United Kingdom

12
13 **Key words:** *caries, remineralisation, silver diamine fluoride, hydroxyapatite, apatite*

14
15 **Correspondence to :**

Prof. C.H.Chu

Faculty of Dentistry

The University of Hong Kong

34 Hospital Road

Hong Kong SAR, China

Tel: +852 2859 0287

Fax: +852 2858 7874

E-mail: chchu@hku.hk

23
24 Prof. A.W.Walls

Edinburgh Dental Institute

Lauriston Building (4th Floor)

Lauriston Place

Edinburgh EH3 9HA

United Kingdom

Tel: +44(0)131 536 4975

Fax: +44(0)131 536 4971

E-mail: angus.walls@ed.ac.uk

34 **Abstract**

35
36
37
38
39
40
41
42
43
44
45
46
47
48
49
50
51
52
53
54
55
56
57
58
59
60
61
62
63

Silver diamine fluoride (SDF) is found to promote remineralisation and harden the carious lesion. Hydroxyapatite crystallisation is a crucial process in remineralisation, however, the role of SDF in crystal formation is unknown. We designed an in vitro experiment using calcium phosphate with different SDF concentrations (0.38 mg/ml, 1.52 mg/ml, 2.66 mg/ml and 3.80 mg/ml) to investigate the effect of this additive on the nucleation and growth of apatite crystals. Two control groups, namely calcium phosphate ($\text{CaCl}_2 \cdot 2\text{H}_2\text{O} + \text{K}_2\text{HPO}_4$ in buffer solution) and SDF ($\text{Ag}(\text{NH}_3)_2\text{F}$ in buffer solution) were also prepared. After incubation at 37°C for 24 hrs, the shape and organisation of the crystals were examined by bright field transmission electron microscopy (TEM) and electron diffraction. Unit cell parameters of the obtained crystals were determined with powder X-ray diffraction (P-XRD). The vibrational and rotational modes of phosphate groups were analysed using Raman microscopy. The TEM and selected-area electron diffraction confirmed that all solids precipitated within the SDF groups were crystalline and that there was a positive correlation between the increased percentage of crystal size and the concentration of SDF. The P-XRD patterns indicated fluorohydroxyapatite and silver chloride were formed in all the SDF groups. Compared with calcium phosphate control, a contraction of the unit cell in the a-direction but not the c-direction in SDF groups was revealed, which suggested that small, localised fluoride anions substituted the hydroxyl anions in hydroxyapatite crystals. This was further evidenced by the Raman spectra, which displayed up-field shift of the phosphate band in all of the SDF groups and confirmed that the chemical environment of the phosphate functionalities indeed changed. The results suggested that SDF reacted with calcium and phosphate ions and produced fluorohydroxyapatite. This preferential precipitation of fluorohydroxyapatite with reduced solubility could be one of the main factors for arrest of caries lesions treated with SDF.

64 **Background**

65 Silver diamine fluoride (SDF) is a topical fluoride solution that has been used for caries
66 management. Unlike other fluoride products which prevent the formation of new caries, SDF is
67 capable of efficiently halting the caries process (Gao et al. 2016). Recently, this caries-arresting
68 property of SDF has drawn much attention from dental clinicians and researchers. SDF has shown
69 its clinical success on arresting the coronal caries of the primary teeth of children (Chu et al. 2002),
70 permanent teeth in teenagers (Chu et al. 2014) and root caries of the elderly (Tan et al. 2010). An
71 *in vitro* study found that SDF increases the mineral density of the artificial carious lesion (Mei et
72 al. 2013b); *ex vivo* studies investigated the collected, exfoliated primary teeth from the SDF clinical
73 trials and found a hardened and highly mineralised zone was formed in the outermost 150 µm of
74 an SDF-treated carious lesion (Chu and Lo 2008; Mei et al. 2014b). Silver has a well-known
75 antibacterial effect and previous studies demonstrated that SDF inhibited cariogenic biofilm
76 formation (Chu et al. 2012; Mei et al. 2013a; Mei et al. 2013c).

77

78 However, there are only a few publications that report the mode of action of SDF on
79 mineralised tissue. Yamaga et al. (1972) suggested that the formation of calcium fluoride (CaF₂)
80 and silver phosphate (Ag₃PO₄) could be responsible for the prevention of dental caries and the
81 hardening of a carious lesion. However, Suzuki et al. (1974) demonstrated the formation of CaF₂
82 by mixing enamel powder with an SDF solution, but the amount of CaF₂ dropped significantly
83 when the materials were immersed into artificial saliva. They also found that Ag₃PO₄ disappeared
84 after being immersed in artificial saliva, and was replaced by silver chloride (AgCl) and silver
85 thiocyanate (AgSCN). In addition, Lou et al. (2011) found a CaF₂-like material and metallic silver
86 were formed by mixing SDF with hydroxyapatite powder and gelatine (as a chemically-
87 representative protein), but the CaF₂-like material dissolved and disappeared after washing with
88 water. Therefore, the mode of SDF action is still unclear.

89

90 The high concentration of calcium and phosphate in saliva is the major mineral source in
91 the oral environment. The contribution of calcium, phosphate and hydroxyl ions present in saliva
92 to apatite deposition is fundamental. However, to the best of our knowledge, there has been no
93 study to investigate the role of SDF as an additive in synthetic apatite crystallisation experiments.
94 It is therefore worthwhile to study mineral structures formed in the presence of SDF to gain insights

95 into these complex reactions (Beniash et al. 2005). Thus, this study aimed to observe the effect of
96 SDF on hydroxyapatite crystallisation occurring *in vitro*, whereby the observed apatite deposition
97 was described using a simplified chemical model. The null hypothesis was that SDF had no effect
98 on crystal formation.

99

100 **Materials and methods**

101 *Mineralisation reaction*

102 The reaction was performed in a Tris-buffered saline (TBS), consisting of a 50 mM Trizma
103 base and 150 mM sodium chloride (NaCl) in Milli-Q water set at pH 7.40. Apatite precipitation
104 was achieved by incubating CaCl₂ (5.88 mM, Merck Ltd., Darmstadt, Germany) with K₂HPO₄
105 (4.12 mM, Merck Ltd., Darmstadt, Germany) in TBS at 37 °C for 24h as described (Habraken et
106 al. 2013), in the presence or absence of different concentrations of SDF: 0.38 mg/ml (fluoride
107 concentration: 45 ppm), 1.52 mg/ml (fluoride concentration: 180 ppm), 2.66 mg/ml (fluoride
108 concentration: 314 ppm) and 3.80 mg/ml (fluoride concentration: 448 ppm). These 4 groups
109 containing SDF were called SDF groups. The calcium phosphate control contained CaCl₂ +
110 K₂HPO₄, but no SDF. The SDF control comprised 0.38 mg/ml SDF in the TBS without
111 CaCl₂·2H₂O + K₂HPO₄. The final pH values of each reaction were measured using a pH electrode.
112 Samples were then analysed using transmission electron microscopy (TEM) with Energy-
113 dispersive X-ray spectroscopy (EDS), powder X-ray diffraction (P-XRD) and Raman
114 spectroscopy (see below). The experiment was done in triplicate.

115

116 *Transmission and scanning electron microscopy analysis*

117 For TEM and EDS analysis, formvar/carbon-coated 200-mesh Ni TEM grids (Agar
118 Scientific, Dorset, UK) were plasma treated for 40 seconds using a Quorum sputter-coater prior to
119 use. The grids were floated upside-down over a 2 ml reaction solution in a 24-well plate. At the
120 end of the reaction, the grids were rinsed with Milli-Q water, blotted against filter paper, air dried
121 and analysed by TEM. TEM Analysis was performed using a Technai F20 (FEI) equipped with a
122 field-emission gun and an 8k × 8k Tietz CCD camera (Beniash et al., 2005). Ten crystal units were
123 selected randomly from the TEM images, and the width and length of the crystal unit was measured
124 using the image analysis software “imageJ” (National Institutes of Health, Bethesda, MD, USA).
125 The changes in proportions of the crystals for each group were calculated based on the difference

126 between the means of each group divided by that of the calcium phosphate control group. Selected-
127 area electron diffraction (SAED) was performed in order to determine the crystallographic
128 parameters of the investigated samples. EDS was used to characterise the chemical composition
129 of the precipitates and quantify the fluoride/calcium (F/Ca) and fluoride/phosphorus (F/P) ratios
130 by dividing the mean atomic percentage of fluoride by either that of the calcium or that of the
131 phosphorus.

132

133 ***Powder X-ray diffraction***

134 The reaction solution was centrifuged at 5,000 g and the pellet was collected and washed
135 thoroughly by Milli-Q water and re-suspended into ethanol. A drop (*ca.* 10 μL) of this suspension
136 was deposited on a low background Si-substrate and the solvent was allowed to evaporate. The
137 samples were then analysed using a Bruker D2 Phaser P-XRD diffractometer equipped with a
138 $\text{CuK}\alpha$ lamp ($\lambda = 1.54056 \text{ \AA}$). Data collection parameters included: 2θ range = $20\text{--}60^\circ$, step size =
139 0.02° and scan speed = 0.5 second/step. Hexagonal unit cell parameters a and c were calculated
140 according to Bragg's equation (1), from the (300)- and (002)- reflections observed in the recorded
141 P-XRD patterns (Liu et al., 2013).

142

$$143 \quad d = \frac{n\lambda}{2 \sin \theta}$$

144

145 (where d – distance between symmetry equivalent diffraction planes, n – consecutive natural number, λ –
146 wavelength, θ -incident angle of the X-ray beam)

148

147 ***Raman spectroscopy***

149 Raman spectra of the samples were recorded using a Renishaw InVia Raman microscope
150 system (3 accumulations, $900 - 1500 \text{ cm}^{-1}$ range) equipped with a 785 nm laser. The laser spot size
151 was approximately $3 \mu\text{m}$, focused on the growth electrode, and the power was kept below 1
152 $\text{mW}/\mu\text{m}^2$. All spectra were recorded at ambient temperature (Chen et al., 2015).

153

154 ***Statistical analysis***

155 The length and width of the crystal were assessed for a normal distribution using Shapiro-
156 Wilk test for normality. One-way ANOVA with Bonferroni post hoc tests were used to detect

157 differences between groups. Analyses were performed with the computer software SPSS Statistics,
158 V19.0 (IBM Corporation, Armonk, USA). The level of statistical significance was set at 0.05.

159

160 **Results**

161 The TEM images revealed the morphology of experimental groups and corresponding
162 SEAD and EDS results. Apatite crystals formed in the absence of SDF exhibited the characteristic
163 plate-shape morphology (Kokubo et al. 2003), SAED showed the typical reflections corresponding
164 to the (211)-, (002)- and (112)- planes of apatite. EDS confirmed the presence of Ca and P (Figures
165 1A-C). The addition of increasing concentrations of SDF to the reaction resulted in a change in
166 the morphology of the crystals, shifting from plate-shaped crystals (no SDF) to round-ended
167 prismatic morphology (Figures 1D-O). SAED showed the reflections corresponding to the (002)-
168 , (211)- and (112)- planes, confirming that these crystals were made of apatite. Furthermore, the
169 recorded EDS spectra contained a signal attributed to fluoride, in addition to Ca and P, confirming
170 that fluoride was present in the investigated apatite samples. Interestingly, as the concentration of
171 SDF increased, the crystals became longer and thicker. The width of the crystals (mean±SD) were
172 14±4nm^①, 33±3nm^②, 79±14nm^③, 117±17nm^④ and 126±6nm^⑤ in calcium phosphate control
173 (no SDF), 0.38mg/ml SDF, 1.52 mg/ml SDF, 2.66 mg/ml SDF and 3.80mg/ml SDF groups,
174 respectively (①<②<③<④,⑤; p<0.001). The length of the crystals (mean±SD) were 137±25^①
175 , 273±72nm^②, 497±55nm^③, 547±94nm^④ and 650±49nm^⑤ in calcium phosphate control (no
176 SDF), 0.38mg/ml SDF, 1.52 mg/ml SDF, 2.66 mg/ml SDF and 3.80mg/ml SDF groups,
177 respectively (①<②<③,④<⑤; p<0.001). Their aspect ratios (width divided by the length) also
178 changed, going from 0.10 to 0.19. There was a positive correlation between the increased
179 percentage of crystal size and the concentration of SDF (Figure 2). The increase in the width was
180 much larger than that of the length, which is reflected in the change in the aspect ratio ($m = 2.20$)
181 that can be found in Figure 2A than that found in Figure 2B ($m = 0.91$). As expected, no
182 hydroxyapatite crystal was detected in the SDF control (no calcium phosphate) group.

183

184 There was a steady increase of both F/Ca and F/P ratios in the crystal when SDF
185 concentration went up (Table 1). The reaction conditions were alkaline in all the SDF groups and
186 the pH values increased when SDF concentrations increased. The pH value measured in the group

187 containing calcium phosphate was 7.07, this drop of pH from the original 7.40 suggested a
188 hydroxyl ion was incorporated into crystal and more hydrogen ions were released (Habracken et al.
189 2013). All of the results indicate the formation of fluorohydroxyapatite in all of the SDF groups,
190 whereby the fluoride content increased with SDF concentration.

191
192 The typical P-XRD pattern of the experimental groups is shown in Figure 3A. The P-XRD
193 analysis indicated that the solids precipitated in the calcium phosphate control group scattered X-
194 rays similarly to hydroxyapatite. However, the reflections in SDF groups were sharper than that in
195 the calcium phosphate control group, in particular in the hydroxyapatite (211)-, and (300)-
196 reflections. It was found that the (300)- reflections in SDF groups were shifted slightly from $\sim 32.3^\circ$
197 (2θ) to $\sim 33.2^\circ$ (2θ) compared to the calcium phosphate control group (Figure 3B). The (002)-
198 reflection was not significantly changed. This pattern of reflection is similar to the one of
199 fluorohydroxyapatite previously reported (Chen et al., 2005). These shifts also reflect the
200 contraction of the calculated unit cell parameters, as summarised in Table 1. Apart from apatite,
201 the strong reflections at 27.88° , 32.28° and 46.28° in the SDF groups and the SDF control group
202 (no calcium phosphate) were coincident with silver chloride (AgCl) (111)-, (200)- and (220)-
203 reflections, which suggested that AgCl precipitated as a separate phase in the SDF-containing
204 samples. Traces of silver oxide were also detected in the 0.38 mg/ml SDF group.

205
206 The Raman spectra showed that all experimental groups displayed a strong PO_4^{3-} band at
207 $\sim 960 \text{ cm}^{-1}$, except for the SDF control (no calcium phosphate) group (Figure 4). The PO_4^{3-} band
208 associated with the P-O stretch shifted from 961 cm^{-1} in calcium phosphate control group (no SDF)
209 to $\sim 965 \text{ cm}^{-1}$ in SDF groups, indicating a change of the phosphate group environment and
210 suggesting – taking into account the composition of the reaction mixture - a substitution of the
211 hydroxyl groups with more electronegative fluoride anions.

212 213 **Discussion**

214 This was the first study which investigated the effect of SDF on remineralisation progress
215 in the context of crystal formation. The null hypothesis was rejected according to the results of this
216 research. SDF clearly altered the crystal structure of the precipitated minerals and its presence

217 enabled the formation of fluorohydroxyapatite. This observation helps to build the understanding
218 of the role of SDF in the remineralisation of caries.

219
220 In this study, we adopted a buffered calcium phosphate system to perform the reaction, this
221 system has been shown to be able to start an initial deposition of amorphous calcium phosphate
222 and favours subsequent transformation into small crystals of apatite and ultimate growth of
223 ripening of those crystals (Termine and Posner 1970). However, this might be different from real
224 situation. Another limitation of the chemical system is the lack of biological component, in which
225 the role of silver could be underestimated. This chemical system is very different from complex *in*
226 *vivo* situation and thus caution should be exercised in data interpretation.

227
228 Although the commercial SDF solution (Saforide) has a high concentration of silver (255,000
229 ppm) and fluoride (448,000 ppm), clinical treatment will consist of a one-time application of a
230 minute volume of the solution (0.22 ± 0.07 mg) to carious lesions (Chu et al. 2012). In the clinical
231 setting, the SDF will be readily diluted by saliva in the oral cavity. The volume of saliva in the
232 mouth is around 0.60 mL (Lagerlöf F and Dawes C, 1984). The concentration of SDF per
233 application is approximately $0.22/0.60$, namely 0.36 mg/ml. Base on this assumption, we arbitrarily
234 selected several concentrations from 0.38 mg/ml to 3.80 mg/ml in this study.

235
236 Saliva plays a crucial role in the caries remineralisation progress. It is a buffered system,
237 supersaturated with respect to calcium phosphate, whereby proline- and tyrosine-rich proteins
238 inhibit the excessive nucleation of apatite phases (Schwartz SS et al. 1992). The salivary activities
239 of calcium and phosphate ions are important because both species are part of the hydroxyapatite
240 unit cell. Therefore saliva offers a protective and reparative environment for teeth. The calcium
241 and phosphate ions provided by $\text{CaCl}_2 + \text{K}_2\text{HPO}_4$ in TBS were a basic simulation of this salivary
242 environment. TEM grids were explicitly floated upside-down during the incubation to prevent the
243 sedimentation of particles formed by homogeneous nucleation on their surfaces (Majewski and
244 Allidi 2006). In this study, we demonstrated that SDF reacted with calcium and phosphate from
245 salivary environment and form fluorohydroxyapatite. Apart from salivary environment, the
246 residual mineral crystals of the tooth could be another important factor of remineralisation, it
247 serves as nucleation site for the newly formed fluorohydroxyapaptite to precipitate (Peters et al.

248 2010), or promotes the ion exchange of F^- for OH^- (Ogard et al. 1994). However, the exchange of
249 the F^- for OH^- requires an acidic micro-environment to dissolve the tooth mineral in order to release
250 OH^- . SDF is very alkaline (pH around 10). This alkaline property matches the favourable condition
251 to synthesis fluorohydroxyapatite in chemistry (Chen and Miao 2005) which may fasten the
252 reaction process by promoting precipitation.

253
254 The hydrogen ions (H^+) of the hydroxyapatite were arranged in the atomic interstices
255 neighbouring the oxygen ions (O^{2-}). The OH^- conferred a certain degree of disorder to the crystal
256 structure of hydroxyapatite (Chen and Miao 2005). An increase in the vibrational frequency of
257 phosphate group in SDF groups was observed in Raman spectra, which indicates the substitution
258 of OH^- with more electronegative F^- (Chen et al. 2015). The isotropic distribution of charge on F^-
259 anions allows for a better fit in the lattice compared to the larger asymmetric OH^- ion (Robinson
260 et al. 2004), thus reducing lattice microstrain and enabling fluorohydroxyapatite crystals to form
261 larger particles. This alternating arrangement produces a fairly well-ordered apatite structure,
262 which is characterised with increased thermal and chemical stability when compared with
263 hydroxyapatite (Chen and Miao 2005). In addition, since F^- is smaller than OH^- , the substitution
264 also results in a noticeable contraction in the a -axis dimensions of the lattice (Table 1) (Liu et al.
265 2013; Wei et al. 2003).

266
267 The P-XRD pattern showed that calcium phosphate control group diffracted poorly (Figure
268 3). It is plausible that the unit cell of calcium phosphate was large and flexible enough to
269 accommodate other matters. This reduced X-ray coherence length and resulted in broader
270 reflections with low intensities. P-XRD relies on Bragg's Law. There is no scattering when there
271 is no d -spacing. In addition, The Ca/P ratio was 1.95 in the 0.38 mg/ml SDF group. However, for
272 the SDF concentrations at or higher than 1.52 mg/ml, the ratios varied between 1.48 and 1.62,
273 which was consistent with apatite minerals. Furthermore, EDS provided a semi-quantitative view
274 of the elemental composition in the inspection field in units of weight/atomic percent. It might not
275 be suitable to determine the precise stoichiometric determination of the ratios between calcium
276 and phosphate in the samples.

277

278 We detected enlarged apatite crystal sizes in the SDF groups and the size of the crystals
279 increased with the increase in SDF concentration. This is consistent with a previous bone study
280 which showed that fluoride uptake is accompanied by an increase in the apatite crystal size (Eanes
281 and Hailer 1998). It is plausible that the introduction of well localised, isotropic, negatively
282 charged F^- increases the stability of the structure and reduces the amount of defects related to the
283 lattice strain. Therefore, single-crystalline domains may grow larger before their growth is
284 interrupted by a crack or irreparable dislocation. We also found that this increase of crystal size
285 took place predominantly in its width but not in its length (Figure 2). Fluoride stabilised
286 preferentially the lateral growth against aberrant outgrowths, thus promoting a more orderly
287 growth of new accretion layers (Eanes and Hailer 1998). The collagen matrix plays an important
288 organisational role in establishing the manner of the crystal arrangements as well as placing some
289 spatial constraints on their size and shape (Eanes and Hailer 1998). Further studies can be
290 performed to address this aspect.

291
292 We did not find CaF_2 , which was probably attributed to the low concentration of SDF used
293 in this study. Other studies found that CaF_2 was not stable (Lou et al. 2011; Suzuki et al. 1974).
294 The amount of CaF_2 significantly dropped after being immersed into artificial saliva (Suzuki et al.
295 1974) or disappeared after washing with water (Lou et al. 2011). Although immersing into artificial
296 saliva or washing with water was to mimic the salivary fluid in clinical situation, this way of rinsing
297 samples after exposure to SDF was susceptible to remove surface precipitation. Ogard et al. (1994)
298 showed that CaF_2 serve as a source of fluoride for the formation of fluorapatite. However, other
299 investigators questioned the formation of CaF_2 within clinically relevant exposure times from
300 concentrated fluoride solutions (Attin et al. 1995, Bruun and 284 Givskov 1993). Attin et al. (1995)
301 showed that 80% of the CaF_2 was lost in 5 days after fluoride varnish application. Bruun and
302 Givskov (1993) reported that CaF_2 (or its likes) was not formed in measurable amounts on sound
303 tooth. It is generally agree that a fluoride-releasing reservoir system is effective at low pH (Ogard
304 et al. 1994; ten Cate 1997). SDF is alkaline. Its mechanism can be different from other acidic
305 fluoride products. We found that SDF played a role incrySTALLISATION and induced the formation of
306 fluorohydroxyapatite. The signature of silver was not detected in the TEM/EDS experiment, which
307 confirms that silver ions do not occlude within the newly formed fluorohydroxyapatite lattice. The

308 only species originating from SDF that clearly had an effect on fluorohydroxyapatite precipitation
309 were the fluoride anions that substituted the hydroxyl ions in the crystal.

310
311 Apart from calcium phosphate, silver chloride is a principal silver product that was detected
312 using P-XRD. This result is consistent with previous studies (Mei et al. 2013b; Suzuki et al. 1974).
313 Silver chloride has a low solubility of 8.9×10^{-5} g/100 ml, which might also contribute to the
314 increased hardness of a carious lesion. Nevertheless, it has been shown that a silver ion has an
315 antibacterial effect against cariogenic bacteria (Chu et al. 2012; Mei et al. 2013a; Mei et al. 2013c)
316 and inhibits the collagenases degrading of dentine collagen (Mei et al. 2014a; Mei et al. 2012).

317
318 In summary, the present study demonstrated that SDF reacts with calcium and phosphate
319 ions and produce fluorohydroxyapatite. This preferential precipitation of fluorohydroxyapatite
320 with reduced solubility could be one of the main factors for arrest of caries lesions treated with
321 SDF.

322

323 **Author Contributions**

324 ML Mei contributed to conception, design, data acquisition, analysis and interpretation and
325 drafted the manuscript; F Nudelman contributed to conception and design and critically revised
326 the manuscript; B Marzec and J Walker contributed to data interpretation and critically revised the
327 manuscript; ECM Lo contributed to conception and critically revised the manuscript; AW Walls
328 and CH Chu contributed to conception, design, data interpretation and critically revised the
329 manuscript. All authors gave final approval and agree to be accountable for all aspects of the work.

330

331 **Acknowledgment**

332 This study was supported by Hong Kong - Scotland Partners in Post-Doctoral Research
333 2015/16 (S-HKU701/15), HKU Seed Fund for Basic Research (No. 201611159029), the
334 Biotechnology and Biological Sciences Research Council (BBSRC, UK) Grant N^o.
335 BB/M029611/1, the Wellcome Trust equipment grant WT087658 and the Scottish Life Science
336 Alliance (SULSA).

337

338 **Conflict of Interest Statement**

339 The research presented in this paper is original. The authors declare no potential conflicts
340 of interest with respect to the authorship and/or publication of this article.

341

342 **References**

- 343 Attin T, Hartmann O, Hilgers RD, Hellwig E. 1995. Fluoride retention of incipient enamel lesions
344 after treatment with a calcium fluoride varnish *in vivo*. Arch Oral Biol. 40(3):169-174.
- 345 Beniash E, Simmer JP, Margolis HC. 2005. The effect of recombinant mouse amelogenins on the
346 formation and organization of hydroxyapatite crystals *in vitro*. J Struct Biol. 149(2):182-190.
- 347 Bruun C, Givskov H. 1993. Calcium fluoride formation in enamel from semi- or low-concentrated
348 f agents *in vitro*. Caries Res. 27(2):96-99.
- 349 Chen JS, Yu ZW, Zhu PZ, Wang JF, Gan ZH, Wei J, Zhao YH, Wei SC. 2015. Effects of fluorine
350 on the structure of fluorohydroxyapatite: A study by XRD, solid-state NMR and Raman
351 spectroscopy. J Mater Chem B. 3(1):34-38.
- 352 Chen Y, Miao X. 2005. Thermal and chemical stability of fluorohydroxyapatite ceramics with
353 different fluorine contents. Biomaterials. 26(11):1205-1210.
- 354 Chu CH, Lee AH, Zheng L, Mei ML, Chan GC. 2014. Arresting rampant dental caries with silver
355 diamine fluoride in a young teenager suffering from chronic oral graft versus host disease post-
356 bone marrow transplantation: A case report. BMC Res Notes. 7:3.
- 357 Chu CH, Lo EC. 2008. Microhardness of dentine in primary teeth after topical fluoride
358 applications. J Dent. 36(6):387-391.
- 359 Chu CH, Lo EC, Lin HC. 2002. Effectiveness of silver diamine fluoride and sodium fluoride
360 varnish in arresting dentin caries in chinese pre-school children. J Dent Res. 81(11):767-770.
- 361 Chu CH, Mei L, Seneviratne CJ, Lo EC. 2012. Effects of silver diamine fluoride on dentine carious
362 lesions induced by streptococcus mutans and actinomyces naeslundii biofilms. Int J Paediatr
363 Dent. 22(1):2-10.
- 364 Eanes ED, Hailer AW. 1998. The effect of fluoride on the size and morphology of apatite crystals
365 grown from physiologic solutions. Calcif Tissue Int. 63(3):250-257.
- 366 Gao SS, Zhao IS, Niraishi N, Duangthip D, Mei ML, Lo EC, Chu CH. 2016. Clinical trials of
367 silver diamine fluoride in arresting caries among children a systematic review. JDR Clinical &
368 Translational Research. 1:201-210.
- 369 Habraken WJEM, Tao JH, Brylka LJ, Friedrich H, Bertinetti L, Schenk AS, Verch A, Dmitrovic
370 V, Bomans PHH, Frederik PM et al. 2013. Ion-association complexes unite classical and non-
371 classical theories for the biomimetic nucleation of calcium phosphate. Nat Commun. 4.
- 372 Kokubo T, Kim HM, Kawashita M. 2003. Novel bioactive materials with different mechanical
373 properties. Biomaterials. 24(13):2161-2175.
- 374 Lagerlöf F, Dawes C. 1984. The volume of saliva in the mouth before and after swallowing. J Dent
375 Res. 63(5):618-21.

- 376 Liu Y, Hsu CY, Teo CM, Teoh SH. 2013. Potential mechanism for the laser-fluoride effect on
377 enamel demineralization. *J Dent Res.* 92(1):71-75.
- 378 Lou YL, Botelho MG, Darvell BW. 2011. Reaction of silver diamine [corrected] fluoride with
379 hydroxyapatite and protein. *J Dent.* 39(9):612-618.
- 380 Majewski PJ, Allidi G. 2006. Synthesis of hydroxyapatite on titanium coated with organic self-
381 assembled monolayers. *Mat Sci Eng a-Struct.* 420(1-2):13-20.
- 382 Mei ML, Chu CH, Low KH, Che CM, Lo EC. 2013a. Caries arresting effect of silver diamine
383 fluoride on dentine carious lesion with *S. Mutans* and *L. Acidophilus* dual-species cariogenic
384 biofilm. *Med Oral Patol Oral Cir Bucal.* 18(6):e824-831.
- 385 Mei ML, Ito L, Cao Y, Li QL, Chu CH, Lo EC. 2014a. The inhibitory effects of silver diamine
386 fluorides on cysteine cathepsins. *J Dent.* 42(3):329-335.
- 387 Mei ML, Ito L, Cao Y, Li QL, Lo EC, Chu CH. 2013b. Inhibitory effect of silver diamine fluoride
388 on dentine demineralisation and collagen degradation. *J Dent.* 41(9):809-817.
- 389 Mei ML, Ito L, Cao Y, Lo EC, Li QL, Chu CH. 2014b. An *ex vivo* study of arrested primary teeth
390 caries with silver diamine fluoride therapy. *J Dent.* 42(4):395-402.
- 391 Mei ML, Li QL, Chu CH, Lo EC, Samaranayake LP. 2013c. Antibacterial effects of silver diamine
392 fluoride on multi-species cariogenic biofilm on caries. *Ann Clin Microbiol Antimicrob.* 12:4.
- 393 Mei ML, Li QL, Chu CH, Yiu CK, Lo EC. 2012. The inhibitory effects of silver diamine fluoride
394 at different concentrations on matrix metalloproteinases. *Dent Mater.* 28(8):903-908.
- 395 Ogard B, Seppa L, Rolla G. 1994. Professional topical fluoride applications--clinical efficacy and
396 mechanism of action. *Adv Dent Res.* 8(2):190-201.
- 397 Peters MC, Bresciani E, Barata TJ, Fagundes TC, Navarro RL, Navarro MF, Dickens SH. 2010.
398 *In vivo* dentin remineralization by calcium-phosphate cement. *J Dent Res.* 89(3):286-91.
- 399 Robinson C, Connell S, Kirkham J, Brookes SJ, Shore RC, Smith AM. 2004. The effect of fluoride
400 on the developing tooth. *Caries Res.* 38(3):268-276.
- 401 Schwartz SS, Hay DI, Schluckebier SK. 1992. Inhibition of calcium phosphate precipitation by
402 human salivary statherin: structure-activity relationships. *Calcif Tissue Int.* 50(6):511-7.
- 403 Suzuki T, Nishida M, Sobue S, Moriwaki Y. 1974. Effects of diammine silver fluoride on tooth
404 enamel. *J Osaka Univ Dent Sch.* 14:61-72.
- 405 Tan HP, Lo EC, Dyson JE, Luo Y, Corbet EF. 2010. A randomized trial on root caries prevention
406 in elders. *J Dent Res.* 89(10):1086-1090.
- 407 Termine JD, Posner AS. 1970. Calcium phosphate formation in vitro. I. Factors affecting initial
408 phase separation. *Arch Biochem Biophys.* 140(2):307-317.

409 Wei M, Evans JH, Bostrom T, Grondahl L. 2003. Synthesis and characterization of hydroxyapatite,
410 fluoride-substituted hydroxyapatite and fluorapatite. J Mater Sci Mater Med. 14(4):311-320.

411 Yamaga R, Nishino M, Yoshida S, Yokomizo I. 1972. Diammine silver fluoride and its clinical
412 application. J Osaka Univ Dent Sch. 12:1-20.

413

414

415 Table 1. Calculated hexagonal unit cell parameters *a* and *c* axes, F/Ca, F/P and final
416 pH, in experimental groups. All the data are normally distributed.

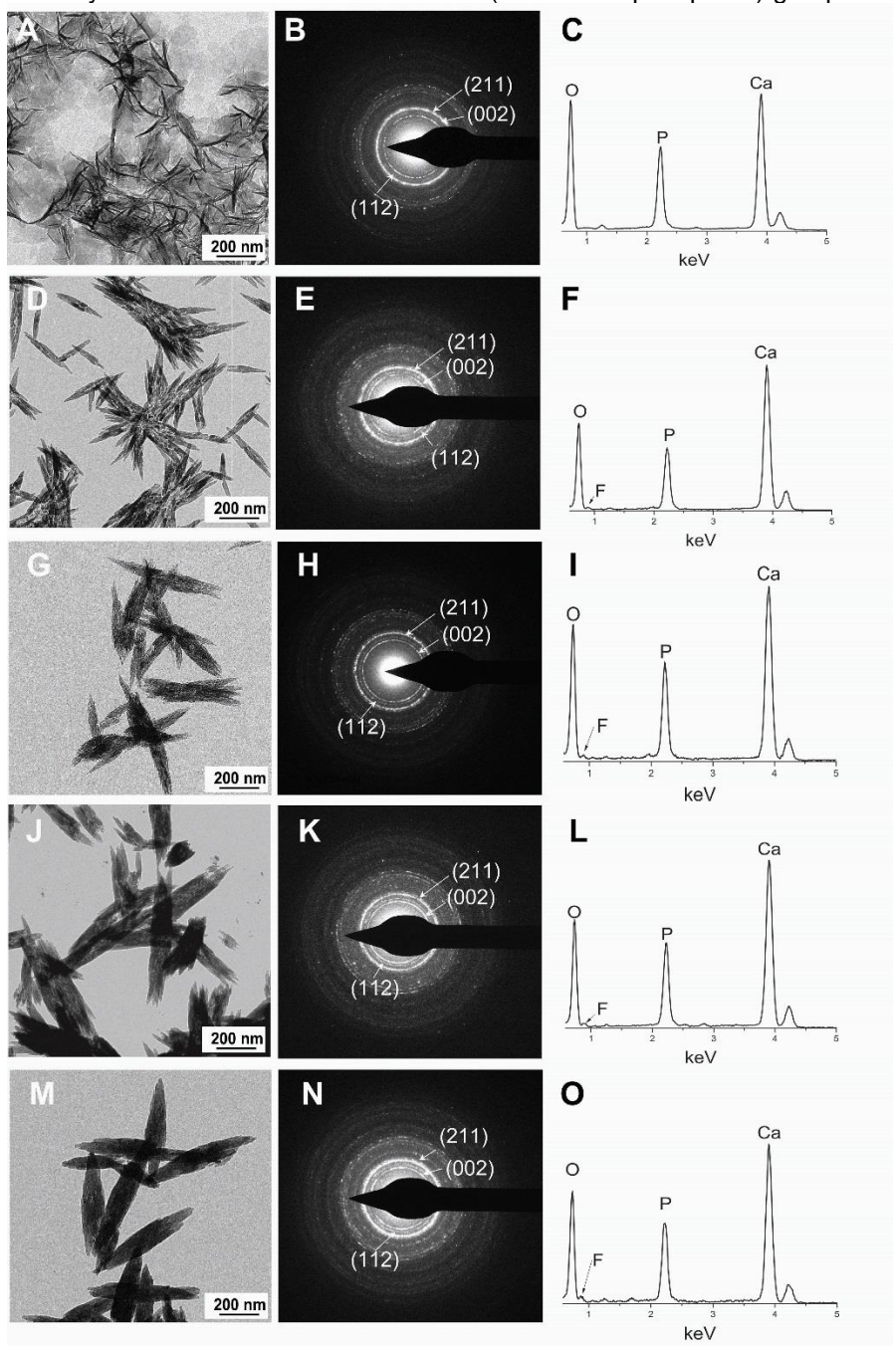
417

Group *	P-XRD		F/Ca	F/P	Final pH
	<i>a</i> -axis (Å)	<i>c</i> -axis (Å)			
No SDF (Calcium phosphate control)	9.577(±0.0012)	6.833(±0.0010)	N/A	N/A	7.07(±0.02)
0.38 mg/ml SDF	9.554(±0.0011)	6.833(±0.0010)	0.022(±0.002)	0.043(±0.006)	8.02(±0.01)
1.52 mg/ml SDF	9.552(±0.0036)	6.833(±0.0010)	0.037(±0.007)	0.055(±0.006)	8.14(±0.01)
2.66 mg/ml SDF	9.548(±0.0024)	6.833(±0.0010)	0.043(±0.004)	0.070(±0.009)	8.60(±0.02)
3.80 mg/ml SDF	9.542(±0.0047)	6.833(±0.0010)	0.072(±0.005)	0.111(±0.011)	8.95(±0.01)

418 * No crystal was detected in the SDF control (no calcium phosphate) group

419

420 **Figure 1. TEM data of experimental groups**
 421 A: Morphology of calcium phosphate control group, B: SAED pattern of calcium phosphate control group;
 422 C: EDS spectra of calcium phosphate control group;
 423 D: Morphology of 0.38 mg/ml SDF group, E: SAED pattern of 0.38 mg/ml SDF group; F: EDS spectra of
 424 0.38 mg/ml SDF group;
 425 G: Morphology of 1.52 mg/ml SDF group, H: SAED pattern of 1.52 mg/ml SDF group; I: EDS spectra of
 426 1.52 mg/ml SDF group;
 427 J: Morphology of 2.66 mg/ml SDF group, K: SAED pattern of 2.66 mg/ml SDF group; L: EDS spectra of
 428 2.66 mg/ml SDF group;
 429 M: Morphology of 3.80 mg/ml SDF group, N: SAED pattern of 3.80 mg/ml SDF group; O: EDS spectra of
 430 3.80 mg/ml SDF group.
 431 * No crystal was detected in SDF control (no calcium phosphate) group



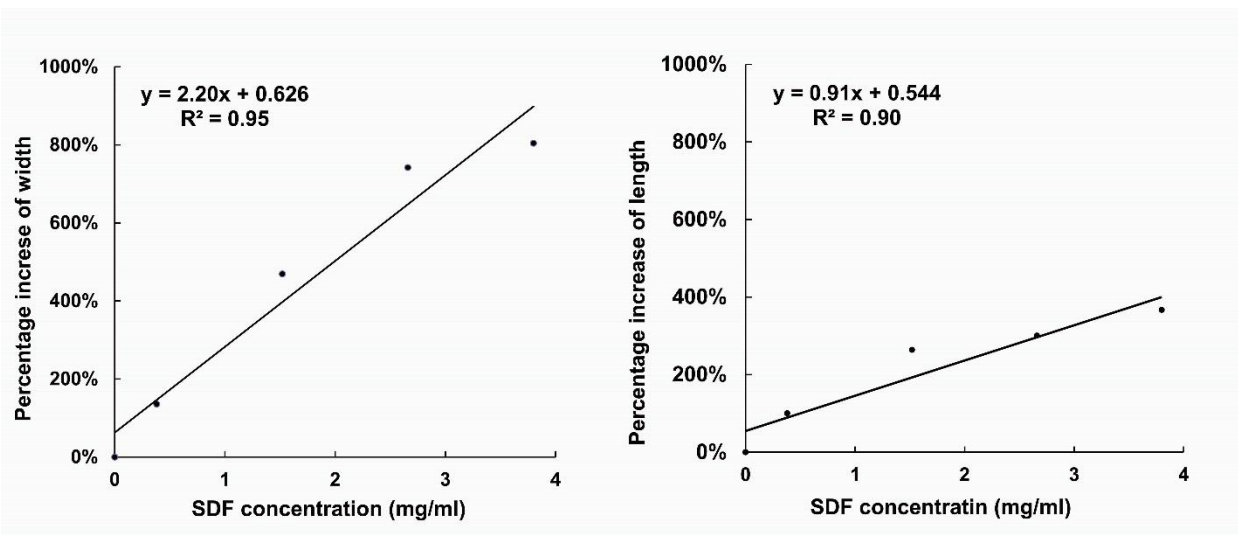
432

433 **Figure 2. Pearson correlation between the percentage increase of crystal size and SDF**
434 **concentrations**

435 A: The correlation between percentage increase of width of crystal and SDF concentration (coefficient $R^2 =$
436 0.95 , slope $m = 2.20$)

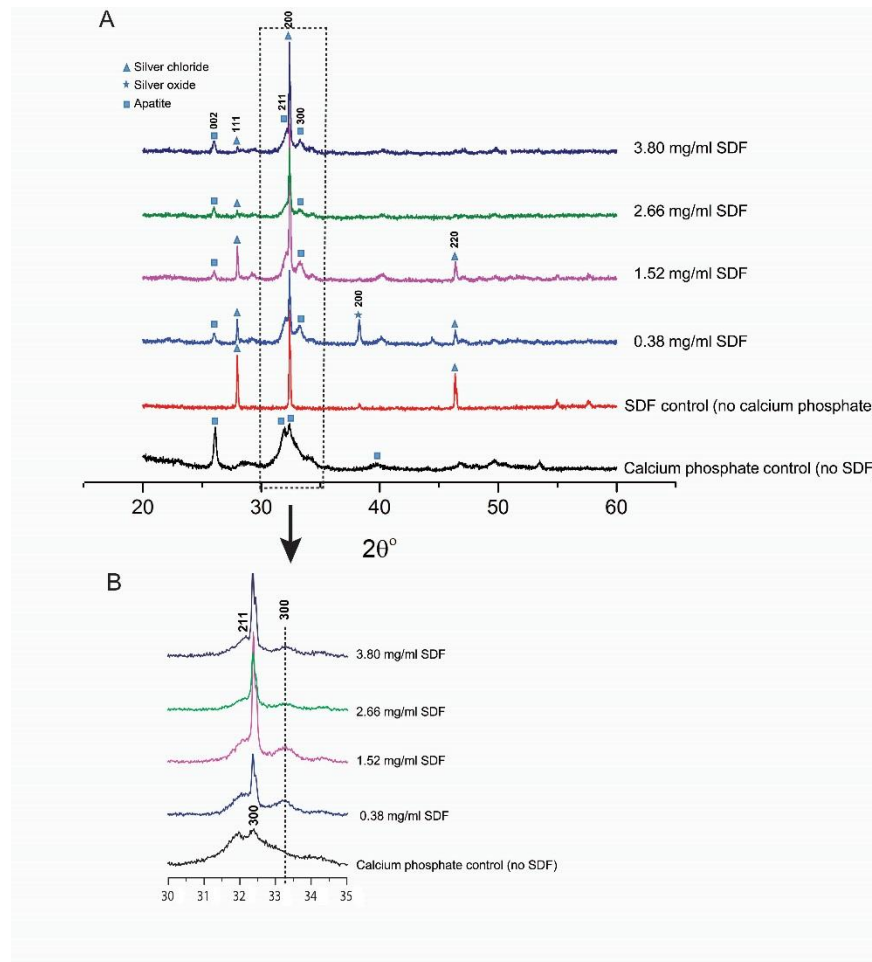
437 B: The correlation between percentage increase of length of crystal and SDF concentration (coefficient $R^2 =$
438 0.90 , slope $m = 0.91$)

439
440



441

442 **Figure 3. Typical P-XRD patterns of the experimental groups;**
443 A: in range of 20 – 60°; B: in range of 30 – 35°

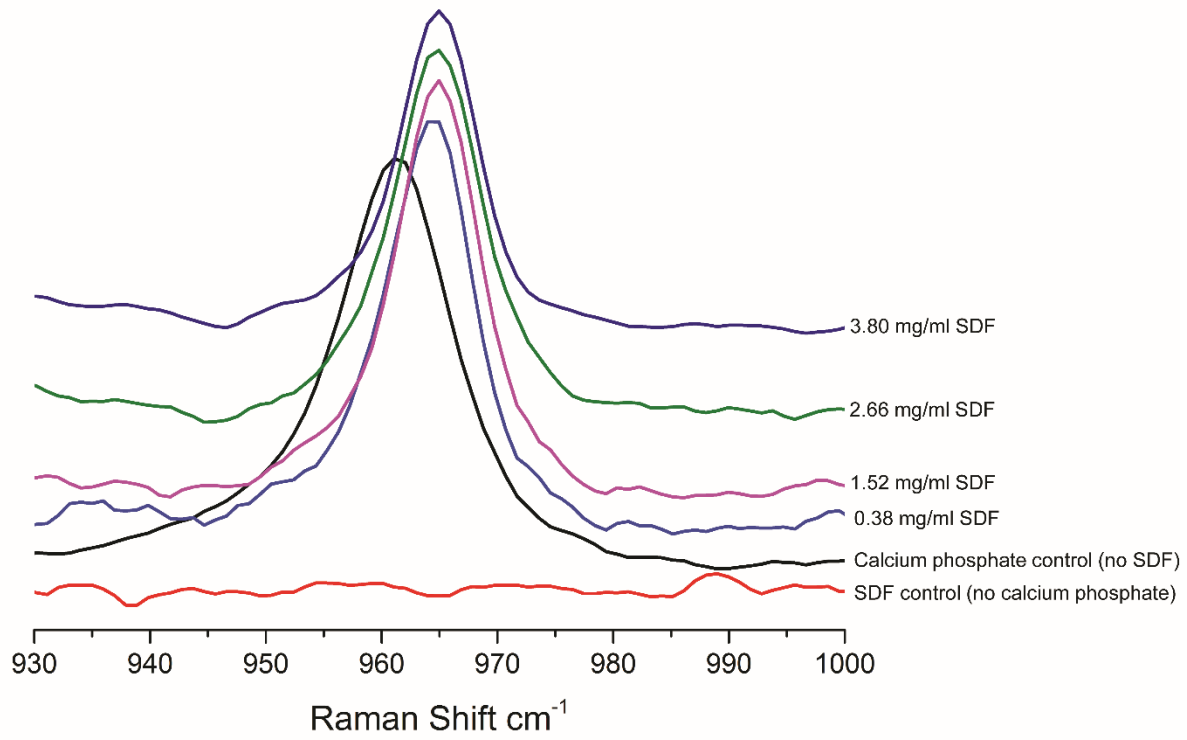


444

445

446

447 **Figure 4. Raman vibrational spectra of the experimental groups in range of 930 –**
448 **1000 cm^{-1}**
449



450
451
452
453
454
455